New Type of Tin(IV) complex based Turn-on Fluorescent Chemosensor for Fluoride ion Recognition: Elucidating the Effect of Molecular Structure on Sensing Property

Journal:	*Dalton Transactions*
Manuscript ID	DT-ART-02-2024-000461.R1
Article Type:	Paper
Date Submitted by the Author:	15-Mar-2024
Complete List of Authors:	Wu, Andrew; Stockton University, Chemistry Hillesheim, Patrick; Ave Maria University, Nelson, Peter; University of the West Indies, Chemistry Zeller, Matthias; Youngstown State University, Department of Chemistry Carignan, Gia ; Rutgers The State University of New Jersey, Chemistry and Chemical Biology Li, Jing; Rutgers The State University of New Jersey, Chemistry and Chemical Biology Ki, Daniel; Stockton University, Chemistry

ARTICLE

New Type of Tin(IV) complex based Turn-on Fluorescent Chemosensor for Fluoride ion Recognition: Elucidating the Effect of Molecular Structure on Sensing Property

Andrew Wu,[a] Patrick C. Hillesheim,[b] Peter N. Nelson,[c] Matthias Zeller,[d] Gia Carignan,[e] and Jing Li,[e] and Daniel W. Ki *[a]

A novel type of chemosensor based on tin(IV) complexes incorporating hydroxyquinoline derivatives has been designed and investigated for selectively detecting fluoride ions. $Sn(meq)_2Cl_2$ (meq = 2-methyl-8-quinolinol) (complex **1**) exhibits a signifcant enhancement in luminescence upon the introduction of fluoride ions. This enhancement greatly surpasses that observed with Snq_2Cl_2 and $Sn(dmqo)_2Cl_2$ (q= 8-hydroxyquinnoline; dmqo=5,7-dimethyl-8-quinolinol). Furthermore, complex **1** displays excellent sensitivity and selectivity for fluoride detection in comparison to halides and other anions. As a result, complex **1** serves as an outstanding turn-on fluorescent chemosensor, effectively sensing fluoride ions. Benesi-Hilderbrand method and Job's plot confirmed that complex **1** associates with F^- in a 1:2 binding stoichiometry. Also, complex **1** exhibited a large binding constant($pK_b=10.4M^{-2}$) and a low detection limit (100 nM). To gain a deeper insight into the photophysical properties and the underlying mechanism governing the formation of the tin(IV) fluoride complex via halide exchange, we successfully synthesized partially fluorinated $Sn(meq)_2F_{0.67}Cl_{1.33}$ (**2**) and fully fluorinated $Sn(meq)_2F_2$ (**3**), all of which were characterized through computational studies, thereby elucidating their photophysical properties. DFT studies reveal that converting $Sn(meq)_2Cl_2$ to $Sn(meq)_2F_2$, an endergonic process, leads to greater stability due to reducing steric hindrance about the metal center. Furthermore, the fluorinated complex significantly increases dipole moment, resulting in high affinity toward F^- ion.

1. Introduction

Developing highly selective and sensitive chemical sensors for the recognition of fluoride ions has emerged as a critical area of research, owing to their pivotal role in addressing environmental, biological, and health-related concerns. Notably, elevated fluoride concentrations in drinking water give rise to public health issues, including dental and skeletal fluorosis, thus underscoring the significance of this research field.[1,2] As a response, the World Health Organization has recommended a stringent guideline of 1.5 mg/L for fluoride content in drinking water.[3,4] The potential adverse effects of excessive fluoride exposure further extend to acute kidney and gastric ailments.[5] Consequently, pursuing highly selective and sensitive chemical sensors tailored to detect fluoride ions has gained prominence and is experiencing continuous growth.

Among the various methods available for fluoride detection, fluorescence-based recognition probes hold particular prominence due to their capacity for rapid, sensitive, and real-time analyte detection. Organic molecule-based luminescent chemosensors have been extensively developed to detect fluoride by exploiting hydrogen bonding interactions, such as thiourea, amide, pyrrolic, imidazole and N-H protonation.[6–12] Alternative approach to detecting fluoride ions involves strong interactions between fluoride ions and Lewis acids, such as silicon and boron.[13–18] This interaction is particularly significant because fluoride ions have a strong tendency to facilitate the cleavage of Si-O and Si-C bonds, attributable to their high affinity for fluoride ions. While these cleavage-based probes provide remarkable selectivity for fluoride detection, they engage in irreversible chemical processes.

Recent advancements have highlighted the advantages of metal complex-based fluorescent chemosensors over their organic molecule-based chemosensors. These metal complexes exhibit superior luminescence quantum efficiency, possess a large Stoke shift, and display redox activity.[19] Moreover, they offer versatile binding sites conducive to anion recognition, encompassing interactions like hydrogen bonding, electrostatic interactions, and coordinative bonding.[20–25] However, most metal complex-based chemosensors lack structural evidence associated with fluoride ions.

a. School of Natural Sciences and Mathematics, Stockton University, Galloway, New Jersey 08205, United States
b. Department of Chemistry and Physics, Ave Maria University, Ave Maria, Florida, 34142, United States
c. Department of Chemistry, The University of the West Indies Mona, Jamaica
d. Department of Chemistry, Purdue University, West Lafayette, Indiana, 47907, United States
e. Department of Chemistry and Chemical Biology, Rutgers University, Piscataway, New Jersey 08854, United States

Our recent research has unveiled interesting phenomena involving tin(IV) halide complexes. Specifically, Sn(IV) chloride complexes undergo halide exchange in the presence of PF_6^- ions, leading to the formation of tin(IV) fluoride complexes, Snq_2F_2 and $Sn(dmqo)_2F_2$ (q=8-hydroxyquinoline; dmqo=5,7-dimethyl-8-quinolinol).[26,27] This halide exchange has intriguing photophysical properties with significantly improved quantum yield and aggregation-induced emission enhancement. Also, the binding of heavier halogens to the tin metal center triggers luminescence quenching behavior due to the promotion of intersystem crossing to an excited state by the spin-orbit coupling of the excited state fluorophore (known as the heavy atom effect).[28–30] These recent findings have opened new avenues for developing potential fluorescent chemosensors tailored to selectively detect fluoride ions in the presence of halides and other types of anions.

Herein, we present a novel "turn-on" fluorescent chemosensor, $Sn(meq)_2Cl_2$ (**1**), designed to detect and recognize fluoride ions among various anions with excellent selectivity and sensitivity. To better understand photophysical properties, we successfully synthesized partially and fully fluorinated complexes (**2** and **3**) via halide exchange. We also introduce and compare a range of other Sn (IV) chloride complexes, evaluating their respective sensing capabilities. DFT studies have also been employed to understand the photophysical properties of tin(IV) complexes toward sensing fluoride ions from a fundamental perspective.

2. Experimental

2.1 Synthesis

Complex **1** was synthesized by a modified and improved procedure of that previously reported by Ngo and Lo.[31] Tin (IV)bis(acetylacetonate) dichloride (0.25mmol, 0.0969g) was mixed with 8-hydroxy-2-methylquinoline (0.5mmol, 0.0795g) and dissolved in 5mL of MeCN in a scintillation vial. The solution was undisturbed for 24 hours before crystals were collected through vacuum filtration. The average percent yield of **1** was determined to be 92%(0.116g). Anal. Calcd for $C_{20} H_{16} Cl_2 N_2 O_2$ Sn: C, 47.48 ; H, 3.19; N, 5.54%. Found: C, 47.34; H,2.95; N, 5.50%. UV–vis, λ_{max} (nm) (ε (dm^3 mol^{-1}cm^{-1})) in MeCN: 257(55876) and 370 (3831). IR-ATR (v/cm^{-1}) for complex **1:** 3063.30(w), 1559.35(w),1426.02(s), 1322.91(m), 1264.43(m), 1103.74(s), 1028.76(w), 836.38(w), 745.91(s), 639.21(w).

Complex **2** was formed by dissolving tin(iv) bis acetylacetonate dichloride (0.25mmol) and 8-hydroxy-2-methylquinoline (0.5mmol) in 4mL MeCN after mixing with ammonium hexafluorophosphate (1.0 mmol) in 3mL H_2O. Single crystals suitable for X-ray diffraction were grown from slow evaporation of a saturated solution of **2** in chloroform. The average percent yield of **2** was determined to be 12%(0.015g). Anal. Calcd for $C_{20} H_{16} Cl_{0.67} F_{1.33} N_2 O_2$ Sn: C, 49.61 ; H, 3.34; N, 5.79. Found: C, 49.66; H,3.22; N, 5.89. UV–vis, λ_{max} (nm) (ε (dm^3 mol^{-1}cm^{-1})) in MeCN: 245(33544), 258(44423), and 366 (3054).

IR-ATR (cm^{-1}) for complex **2:** 3064.36(w), 1945.52(w), 1563.59(w), 1502.95(w), 1425.04(s), 1325.78(m), 1267.03(m), 1103.71(m), 1029.90(w), 836.65(w), 746.34(s), 639.88(w).

Complex **3** was synthesized by dissolving tin(IV)bis (acetylacetonate)dichloride (0.25mmol, 0.969g) and 8-hydroxy-2-methylquinoline in 4 mL of MeOH. 1.0 mmol of ammonium hexafluorophosphate was dissolved in 3 mL of H_2O. The two solutions were combined and undisturbed for 48 hours before crystals were collected through vacuum filtration. The average percent yield of **3** was determined to be 56%(0.067g). Single crystals suitable for X-ray diffraction were grown from the slow diffusion of hexanes into a saturated solution of **3** in chloroform. Anal. Calcd for $C_{20} H_{16} F_2 N_2 O_2$ Sn: C, 50.78 ; H, 3.41; N, 5.92. Found: C, 50.60; H,3.17; N, 5.87. UV–vis, λ_{max} (nm) (ε (dm^3 mol^{-1}cm^{-1})) in MeCN: 244(37714), 262(20294), and 367 (1612). IR-ATR (v/cm^{-1}) for complex **3:** 3059.35(w), 1566.35(w), 1504.30(w), 1426.77(m), 1324.28(m), 1264.39(m), 1108.01(m), 1035.81(w), 838.14(w), 744.23(s), 629.62(w).

Experimental and simulated PXRD patterns for compounds (**1-3**) are presented in Fig.S1.

2.2 Characterizations

2.2.1 X-ray Data Collection and Structure Determinations

Single crystals of compounds **2** and **3** were coated with Parabar 10312 oil and transferred to the goniometer of a Bruker Quest diffractometer with Mo Kα wavelength (λ = 0.71073 Å) and Cu Kα wavelength (λ = 1.54178 Å) and a Photon II area detector. Examination and data collection were performed at 150 K. Data were collected, reflections were indexed and processed, and the files were scaled and corrected for absorption using APEX3, SAINT, and SADABS.[32,33]

For all compounds, the space groups were assigned using XPREP within the SHELXTL [34]suite of programs, and the structures were solved by direct methods using ShelXS or ShelXT [35]and refined by full matrix least squares against F^2 with all reflections using Shelxl2018 using the graphical interfaces Shelxle [36]and/or Olex2.[37] H atoms were positioned geometrically and constrained to ride on their parent atoms. C-H bond distances were constrained to 0.95 Å for aromatic and alkene C-H moieties, and to 0.99 and 0.98 Å for aliphatic CH_2 and CH_3 moieties, respectively. Methyl H atoms were allowed to rotate, but not to tip, to best fit the experimental electron density. U_{iso}(H) values were set to a multiple of U_{eq}(C) with 1.5 for CH_3 and 1.2 for C-H and CH_2 units, respectively.

2.2.2 Quantum Yield

Internal quantum yield (IQY) measurements were made on C9920–02 absolute quantum yield measurement system (Hamamatsu Photonics) with 150 W xenon monochromatic light source and 3.3 in. integrating sphere. Samples for internal quantum yield measurements were prepared by spreading fine powder samples evenly on the bottom of a quartz sample holder. Sodium salicylate (S.S.) was chosen as the standard with a reported IQY value of 60% at the same excitation wavelength (360 nm). Photoluminescence (P.L.) measurements were carried out at room temperature on a Horiba Duetta fluorescence spectrophotometer. Powder samples were evenly distributed and sandwiched between two quartz slides for room

temperature measurements. Both excitation and emission spectra were collected.

Relative quantum yield for complexes **1-3** were measured relative to quinine sulfate(Φ_{std}=0.54) in H_2SO_4 (0.05M) solution using an equation, $\Phi_s = \Phi_{std}(Grad_s/Grad_{std})(\eta_s^2/\eta_{std}^2)$, where the subscript s and std denote sample and standard respectively, Φ is the fluorescence quantum yield, Grad is the gradient from the plot of integrated fluorescence intensity vs absorbance, and η is refractive index of the solvent.[38]

2.2.3 Molecular Modelling

DFT calculations, conducted using a Gaussian 16 software package[39], were carried via the Pople style triply split valence basis set 6-311++G(d,p), whereas Becke's three parameter hybrid function (B3) [40] was employed for fermion exchange, coupled with Lee, Yang and Parr's (LYP) correlation function, of-course augmented with a coulomb attenuating method [41]for better estimation of long range and charge transfer interactions: CAM-B3LYP[42]. Calculations involving Tn(II) were carried out *via* Las Almos National Laboratory's double zeta Effective Core Potential (ECP): LANL2DZ.[43]

3. Results and discussion

3.1 Description of Crystal Structures.

Crystals of $Sn(meq)_2F_2$ (**3**) were formed in the presence of NH_4PF_6, which undergoes hydrolysis to produce $[PO_2F_2]^-$/ F^- or $[PO_3F]^{2-}$.[44–46] The hydrolysis of hexafluorophosphate converts $Sn(meq)_2Cl_2$ to $Sn(meq)_2F_2$ *via* halide exchange as described in our previous work. A partially fluorinated derivative (complex **2**) is formed as an intermediate in the complete conversion of the chlorinated to the fluorinated analogue. The crystal structures of complexes **2** and **3** display a distorted octahedral geometry (Fig. 1) around the tin metal center, where the bond distances and angles surrounding the metal cation fall within
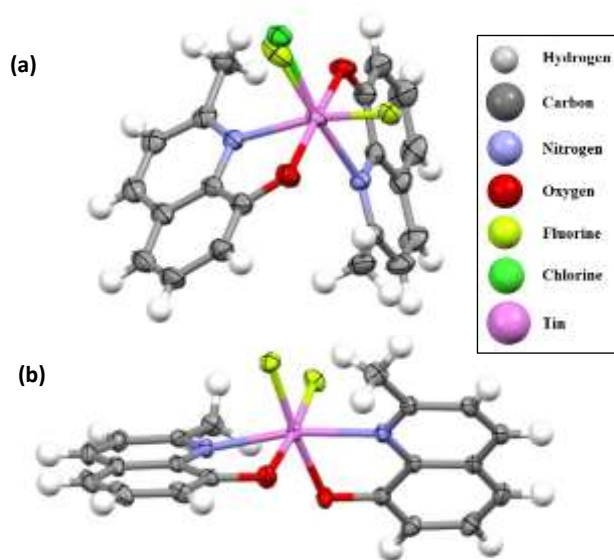

(a)

(b)

Fig. 1. The asymmetric units of compounds complex **2** (a) and complex **3** (b) shown with 50% probability ellipsoids.
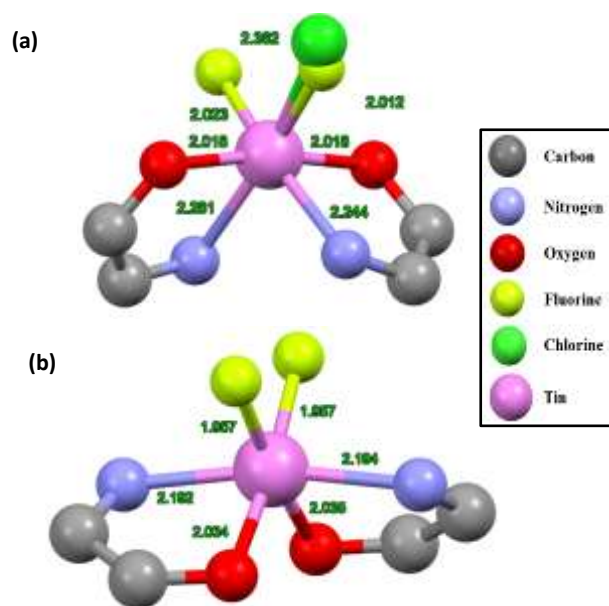

Fig. 2. Depictions of the coordination geometry of the tin metal in compounds **2** (**a**) and 3 (**b**). Bond distances are shown in green (Å). The distances to the disordered chloride and fluoride are both shown in complex 2 (a)

the expected ranges, matching closely with previously reported structures bearing quinolone-based ligands both from our group and from others(see Fig. 2).[26,27,47–49] For complex **2**, the asymmetric unit has a disordered metal coordination geometry with one of the coordination sites on the metal being partially occupied by a chloride and fluoride atom at an approximate 67% and 33% ratio, respectively (Fig. 1).

With respect to crystal structure formation and interactions, the halide moieties on both molecules act as bridges, linking multiple coordination complexes together through H···X (Cl or F) non-covalent interactions. This is observed despite the changes in geometries of the meq ligands (i.e., cis vs trans) as well as the presence of chloride vs fluoride moieties. Depictions of these interactions are shown in the supporting information (Fig. S2). Additionally, both compounds display parallel offset π-stacking. The stacking interactions are distinct when contrasting the two structures. For example, within complex 3, each of the meq ligands displays a unique set of π stacking interactions wherein both aromatic moieties of the meq ring are overlapping. These π interactions form a dimer, of sorts, stabilized in part by these π stacks. In complex 2, however, only one of the rings forms a stacking interaction with the symmetry adjacent meq ligands, forming an extended chain of the metal complexes through these π interactions (Fig. S3).

Optimization of all chemical species involved in the evolution of 1 to yield the difluoride analogue (3) was carried out, revealing, on the basis of the absolute free energies, that.the fluorinated derivative was the most stable, whereas the chlorinated analogue is the most unstable (Fig. 3). However, the forward reaction free energy changes (ΔGxc) at both steps during the exchange process are endergonic.

The energetics of this process for 1 was also compared to those for Snq_2Cl_2 and $Sn(dmqo)_2Cl_2$, revealing conservative ΔGxc values: 42 – 47 kJ mol-1, which suggest that these

transformations should proceed relatively quickly at room temperature, as confirmed by the experimental observations.
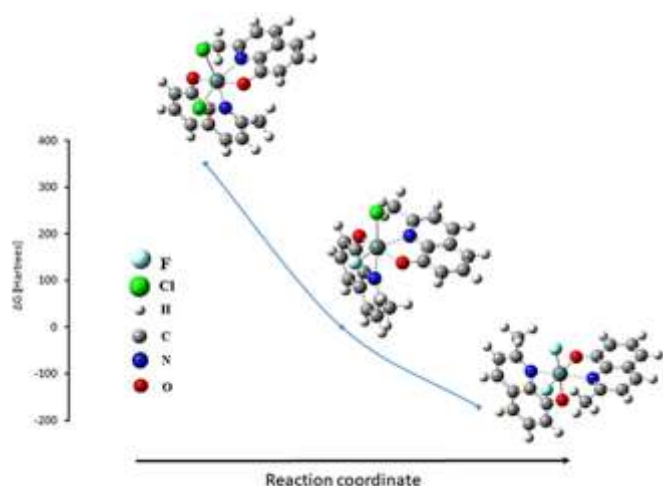

Fig. 3. Free energy change of halide exchanging from Cl to F

Interestingly, of all three compounds, ΔG_{xc} is the most conservative for Sn(meq)$_2$Cl$_2$; for the conversion **1** to **2**, the energy requirement is ca. 43 kJ mol^{-1}. However, for the conversion of **2** to **3**, the process requires only 23.21 kJ mol^{-1}. These forward reaction potentials are most likely caused by steric effects associated with the methyl substituent, which offers considerable resistance to coordination at the ring-based nitrogen binding site. Unfortunately, despite several attempts, transition state searches were unsuccessful; however, these searches reveal that the halogen exchange process involves excessive lengthening of the Sn-N bond as the Sn-F bond order increases at the expense of the Sn-Cl interaction. Indeed, such significant rearrangement is confirmed by the crystal structures of **2** and **3**, where the O-Sn-O arrangement changed from *trans* in the former to *cis* in the latter; a rearrangement which is only feasible if there is complete disconnection at one coordination point during the exchange process.

Nonetheless, since these values are most conservative for Sn(meq)$_2$Cl$_2$, it is reasonable to expect greater sensitivity towards F$^-$ ions, a feature discussed later (*vide infra*). For Snq$_2$Cl$_2$, ΔG_{xc} values are slightly more endergonic for both exchange processes (ΔG_{xc} = 45.56 and 46.50 kJ mol^{-1}), indicating lower relative stability of Snq$_2$F$_2$ product; values which are similar to those calculated for Sn(dmqo)$_2$Cl$_2$ derivative (ΔG_{xc} = 46.10 and 47.05 kJ mol^{-1}). These results indicate that the exchange mechanism is most likely similar for all three starting (chloro-) derivatives. However, differences in the electronics of the final product, caused by changes in the coordination structure, result in different ΔG_{xc} values.

3.2 UV-Visible Spectra and Luminescence Studies
The UV-Vis spectra of complex **1**-**3** were recorded and subjected to analysis in MeCN, as shown in Fig. 4(a). Absorption spectra for complexes **2** and **3** displayed two prominent bands at 245 and 260 nm, respectively, corresponding to π -π* transition of the conjugated ligand and a weak broad peak at 370 nm, assigned to n-π* transition of the conjugated ligand. In the case

of complex **1**, a strong band at 257 nm was observed, along with a weak broad band at 370 nm, both assigned to the π -π* transition and n-π* transition, respectively.[50,51]
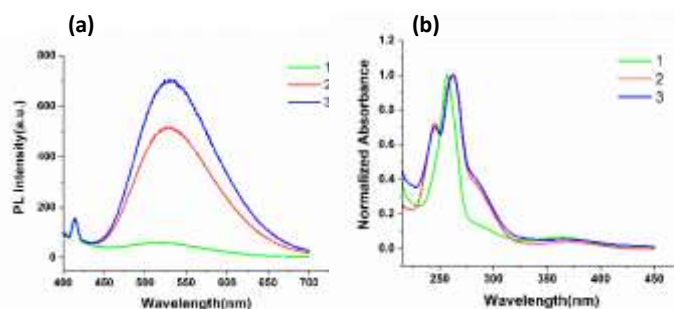

Fig. 4. (a) FL emission spectra of the complexes **1-3** at 1.0 ×10^{-5}M in MeCN solution (λ_{ex}:370nm) (b) Absorption spectra of the complexes**1-3** at 1.5 ×10^{-5}M in MeCN solution

For a more fundamental understanding of these absorptions, time-d ependent DFT calculations were carried out for all complexes, revealing three absorptions in all cases. However, the two absorptions at lowest energy are quite close: ca. 324 and 327 nm, indicating that they might exist as a single band under experimental conditions, in some cases, when explicitly solute-solvent interactions are significant. Secondly, the known insufficiency of DFT methods in accurately estimating degeneracy between closely spaced absorptions might be the reason for the calculated separation of these two bands. Nonetheless, the energetic proximity of these bands to that observed experimentally at 370 nm for this compound indicates correspondence, whereas that calculated at 278 nm is most likely related to that observed experimentally at 257 nm.
Such energetic differences between the calculated and experimental bands are most likely associated with the neglect of explicit solvation by the applied solvent model (*vide supra*).

Based on these results, both of the aforementioned experimental bands are composed of multiple transitions, the majority of which are due to π to π* electron density rearrangement. For instance, in the case of complex **1**, the absorption at highest energy is composed of three transitions: HOMO to LUMO (3.7 %), HOMO to LUMO+1 (49.9 %), and HOMO-1 to LUMO+1 (2.1 %), all of which are associated with electron density migration from the π to π* molecular orbitals (MO). However, whereas the absorption at lower energy is mainly composed of transitions emanating from π to π* electron density rearrangement, there is some amount of n to π* contribution, most of which is reflected in the HOMO-1 to LUMO+4 transition (Fig.5). For complex **2** and **3**, three bands were also calculated. Similar to **1**, the lowest energy bands, as calculated, are highly similar in energy. However, as confirmed by the experimental observations, these two are non-degenerate. The composition of the absorptions of **2** and **3** are summarized in Table 1, and the MO collected is in Fig. S4.

The fluorescence emission spectra showed distinct photophysical properties among Sn(*meq*)$_2$Cl$_2$ (**1**), Sn(meq)$_2$F$_{0.67}$Cl$_{1.33}$(**2**), and Sn(*meq*)$_2$F$_2$(**3**).

Dalton Transactions

λ = 324.17 nm ·······►
λ = 327.60 nm —··—►
λ = 278.0 nm ——►
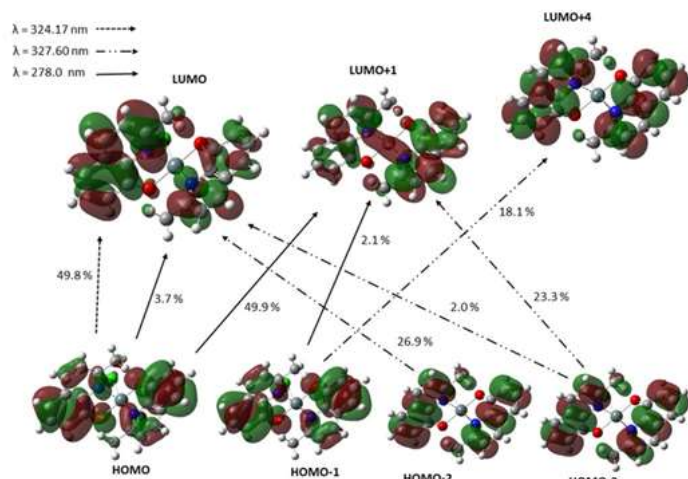
Fig. 5. Calculated MO surfaces for Sn(meq)$_2$Cl$_2$ (compound **1**)

emission of complex **3** in the solid state was blue-shifted relative to that in the solution (Fig. S5). AIE-active materials bear significant promise for organic light-emitting diode (OLED) applications because most phosphor materials experience emission quenching in solid states, decreasing device efficiency.

3.3 Fluoride ion recognition of complexes 1 and 2 among anions.

The influence of fluoride ions on the luminescence and absorption of complexes **1** and **2** was examined through titration with tetrabutylammonium fluoride (TBAF) in CH$_3$CN. Upon the addition of fluoride ions, complex **1** exhibited a substantial increase in fluorescence intensity, presenting it as a potential "turn-on" fluorescent sensor for fluoride ions. As depicted in Fig. 6 (a), the emission spectra of compound **1** exhibited a gradual rise with increasing F$^-$ concentration, eventually plateauing at approximately 1.7 equiv. of F$^-$. The inset graph illustrates the normalized changes in emission intensity at 530 nm as a function of F$^-$ concentration. This enhancement stemmed from the specific binding of fluoride to

Table 1. Calculated absorptions and the constituent transition for all three tin (IV) complexes.

Compound	Transitions		
1	λ = 278 nm HOMO to LUMO (3.7 %) HOMO to LUMO+1(49.9 %) HOMO-1 to LUMO+1(2.1%)	λ = 324.17 nm HOMO to LUMO (49.8 %)	λ = 327.60 nm HOMO-1 to LUMO+4 (18.1 %) HOMO-2 to LUMO (26.9 %) HOMO-3 to LUMO+1 (23.3%) HOMO-3 to LUMO (2.0%)
2	λ = 278.35 nm HOMO to LUMO+2 (23.3 %) HOMO-1 to LUMO+3(8.3 %) HOMO-3 to LUMO(48.7%)	λ = 323.98 nm HOMO to LUMO+1(36.3 %) HOMO-1 to LUMO (6.2 %) HOMO-1 to LUMO+1(43.9%)	λ = 328.68 nm HOMO to LUMO(49.6 %) HOMO to LUMO+1 (9.0 %) HOMO-1 to LUMO+1(9.0%)
3	λ = 279.12 nm HOMO-3 to LUMO (24.6 %) HOMO-1 to LUMO+2(22.3%)	λ = 334.53 nm HOMO to LUMO+1 (53.2 %) HOMO-1 to LUMO (45.2%)	λ = 339.13 nm HOMO to LUMO (55.1 %) HOMO-1 to LUMO+1(43.7%)

The coordination of fluorine to tin(IV) significantly enhanced their luminescence. As illustrated in Fig. 4(b), complex 3 exhibited a luminescence increase of over tenfold compared to complex **1**. This phenomenon is likely attributed to the stronger σ bonding of Sn-F compared to Sn-Cl, a connection drawn from our prior research findings.[27] Intermediate compound **2**, a partially fluorinated complex, also displayed a noteworthy increase, although less pronounced than the fully fluorinated compound **3**. The luminescence quantum yields of complexes **1**, **2**, and **3** were compared in solution and in the solid state. The relative quantum yields in solution were low: 0.1% for complex **1**, 0.7% for complex **2**, 1.3% for complex **3**. These outcomes feature the remarkable impact of fluorination on enhancing complex luminescence. The quantum yields increased significantly in the solid state, reaching 2.5% for complex **1**, 5.8% for complex **2**, and 15% for complex **3**. These observations indicate that the complexes exhibit aggregation-induced emission (AIE) behavior—displaying poor emission in solution yet strong emission in the solid state. [52–54] Interestingly, the FL

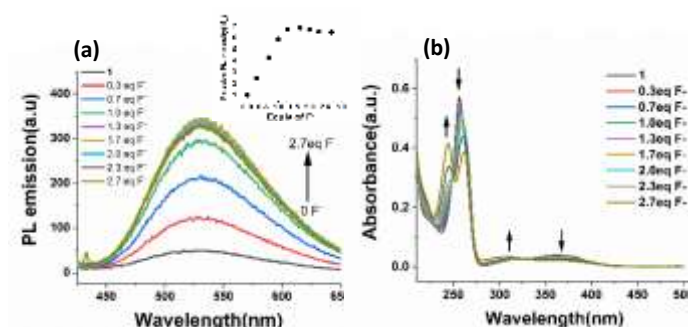the tin(IV) metal center, displacing the chloride ligands.

Fig. 6. FL emission spectra (λ$_{ex}$=370nm) (a) and absorption spectra (b) of complex **1** (1.0×10^{-5} M in MeCN) upon the addition of tetrabutylammonium fluoride (TBAF, 1.0×10^{-3} M in MeCN) Inset: fluorescent titration profile at 530 nm ranging from 0 to 2.7equiv. of fluoride ions.

Consequently, a more stable Sn(IV) fluoride complex formed, benefiting from a lower enthalpy of formation due to the

stronger Sn-F bond (467 kJ/mol) compared to the Sn-Cl bond (410 kJ/mol).[55]

The Benesi-Hildebrand plot of $1/(I-I_o)$ against $1/[F^-]^2$ shows a linear relationship(R^2=0.9935), indicating that complex **1** is bound to fluoride ion in 1:2 stoichiometry(Fig. S6).[56–59] Furthermore, the result of Job's plot indicated that the binding stoichiometry between complex **1** and F^- was 1:2 (Fig. S7). This is reasonable because complex **1** offers two chlorine binding sites. The average binding constant (pK_a) was determined to be 10.4 (M^{-2}), which represented the large affinity for fluoride and complex **1**. This value is comparable to molecular-based fluorescence sensors for fluoride or exceeds that of other metal complex-based chemosensors.[22,57,60,61] The corresponding detection limit of complex **1** was also calculated based on fluorescence and reached 1.0×10^{-7} mol/L (Fig. S8).

The UV-Visible titration of complex **1** with F^- revealed a steady increase in the absorption band at 245 nm and a steady decrease in the absorption band at 260 nm. The distinctive absorption peak at 245 nm signifies the presence of fluorinated complexes, indicating the formation of Sn-F bonds. Isosbestic points within the spectra suggest an equilibrium state between Sn-Cl and Sn-F within the solution.
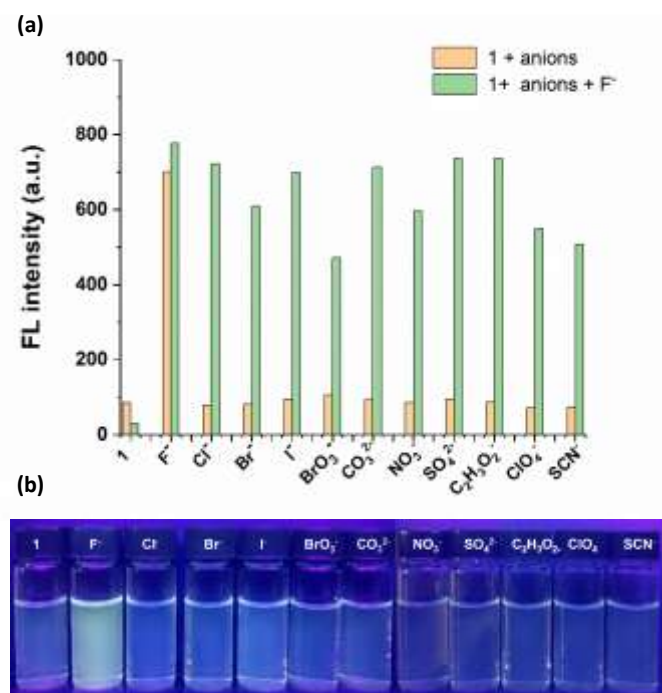
(a)

(b)

Fig. 7. (a) FL emission intensity changes of complex **1** in the presence of anions. 2 equiv.of anions (1.0×10^{-3}M) and for **1** (1.0×10^{-5}M) in MeCN solution were used. (b) photographed image observed after the addition of anions (2 equiv.) to complex **1** (1.0×10^{-5}M) under UV-lamp (360 nm)

Complex **2**, a partially fluorinated, can also function as a responsive "turn-on" sensor for fluoride ions. As displayed in Fig. S9(a), fluorescence emission of complex **2** increases gradually with increasing F^- concentration, saturating at approximately 1.0 equiv. of F^-. This saturation point is attained earlier than in complex **1** due to the partial fluorination of

complex **2**. The absorption behavior of complex **2** aligns with that of complex 1 (Fig. S9(b)).

The selectivity of compounds **1** for fluoride ions was evaluated by measuring their fluorescence emission in the presence of halides and seven other anions, namely BrO_3^-, CO_3^{2-}, NO_3^-, SO_4^{2-}, CH_3COO^-, ClO_4^-, and SCN^-(see Fig.7(a)). The addition of F^- to complex **1** induces a distinctive change in luminescence emission, whereas the other halides and anions cause slight changes. Additionally, competition experiments were conducted to confirm the selectivity of complex **1**. The results indicated that the majority of the anions had a negligible impact on fluoride ion sensing, while two anions, BrO_3^- and SCN^-, exhibited more pronounced quenching compared to others, suggesting potential interference between these anions. On the other hand, it was observed that complex **2** did not exhibit significant selectivity towards fluoride ions compared to the other anions. The bottom of the photo image (Fig. 7(b)) clearly demonstrates that complex **1** produces a strong green emission under UV-lamp (365nm) for complex **1** after the addition of F^-. Consequently, complex **1** demonstrates excellent fluoride ion selectivity among other tested anions. This selectivity is attributed to its unique binding sites (specifically, Cl bound to the metal), which have the capacity to displace with F^- ions through halide exchange.

3.4 Exploration of fluoride ion recognition studies using tin(IV) complexes with hydroxyquinoline derivatives.

We conducted a comparative study of two other tin(IV) chloride complexes, Snq_2Cl_2 and $Sn(dmqo)_2Cl_2$, to investigate their photophysical properties and understand how the electron-donating group influences recognition sensing properties. Our previous research motivated this study, which revealed similar optical properties between these complexes.
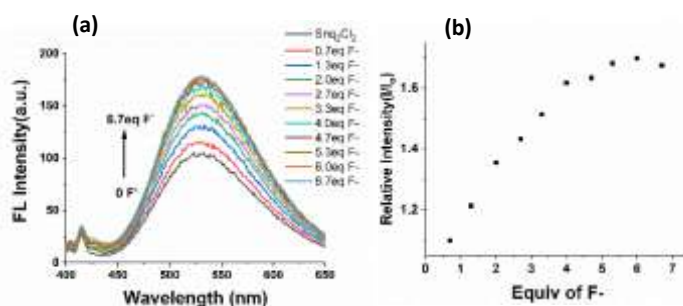
(a) **(b)**

Fig. 8. FL emission spectra upon the addition of tetrabutylammonium fluoride (1.0×10^{-3}M in MeCN) in Snq_2Cl_2 (1.0×10^{-5}M in MeCN) (λ_{ex}=370nm) (a) and relative FL emission(I/I_o) at 530 nm against concentration of fluoride ions (b)

Upon incremental addition of F^- ions to Snq_2Cl_2 in MeCN, we observed a fluorescence emission enhancement, as shown in Fig. 8. The fluorescence intensity gradually increased and reached saturation after introducing 6.0 equivalents of F^- ions to the complex solution, indicating Snq_2Cl_2 requires a higher F^- concentration to attain maximum emission than complex **1** (Titration absorption curves in Fig. S10). The calculated average binding constant (pK_b) was determined to be 9.6 using the

ARTICLE

Benesi-Hildebrand plot with 1:2 stoichiometry and also Job's plot indicated that the binding stoichiometry between Snq_2Cl_2 and F^- was 1:2 (Fig. S11 and S12). This value is lower than that of complex **1**, suggesting that Snq_2Cl_2 exhibits a weaker binding affinity for F^- ions than complex **1**. Consequently, Snq_2Cl_2 displays less sensitivity to F^- ions, as indicated by the slopes of the linear ranges (Fig. 9). Snq_2Cl_2 can act as an F^- sensor by increasing its FL emission signal, but less sensitive compared with complex **1**. Complex **1** is highly responsive to fluoride ions among others. The selectivity of Snq_2Cl_2 was evaluated similarly, and Snq_2Cl_2 shows decent F^- sensing ability along with BrO_3^- as shown in Fig. S13. Interestingly, $Sn(dmqo)_2Cl_2$ demonstrated negligible changes in FL emission upon the addition of F^- ions or other anions, indicating its inactivity as an F^- sensor. Overall, complex **1** exhibits a highly selective and sensitive probe for the recognition and detection of fluoride ions.

In order to gain deeper insights into the photophysical properties, DFT studies were performed by optimizing structures and calculating the energies for the various complexes, revealing dipole moments of ca. 18.0, 17.3, and 17.6 D for complexes **1**, **2**, and $Sn(dmqo)_2Cl_2$, respectively. Upon complete fluorination, these values changed to 91.4, 16.3, and 16.6 D.
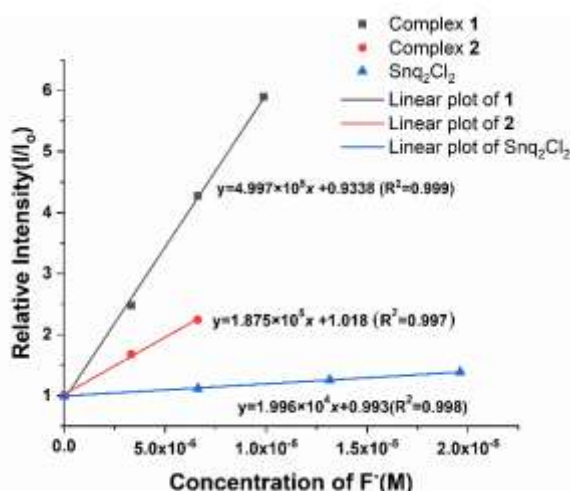

Fig. 9. The sensitivity (the slope of calibration curve) of complexes **1** and **2** and Snq_2Cl_2 by using FL emission intensity change at 530 nm toward various concentrations of fluoride ions in the linear ranges in MeCN solution.

Clearly, the observed sensitivity of **1**, as demonstrated by enhancing FL intensity in the presence of F^- ions, stems from changes in its electronic structure to allow improved change transfer probability. Conversely, other complexes showed the opposite trend. These changes likely arise from variations in the metal center's bonding structure; for instance, fluorination transforms the oxygen binding sites from a *trans* conformation in complex **2** to a *cis* arrangement in **3**. These significant structural alterations impact metal-ligand interactions and electron density in vicinity of the metal. Furthermore, the optimized structures confirm that the O-Sn distances in complex **1** are much shorter since the oxygen atoms adopt a trans arrangement, resulting in less repulsive effects in the bonding around the metal center (Fig. S14). However, in the difluoride complex, the oxygen atoms adopt a *cis* conformation, resulting in greater repulsive effects about the metal center, and longer Sn-O distances. These effects result in a more stable fluoride complex, hence, the observed greater reactivity of **1** toward fluoride ions.

4. CONCLUSIONS

In this study, we explored a novel class of fluorescent tin(IV) complex-based chemosensors designed for the selective detection of fluoride ions among halides and other anions. Notably, complex **1** exhibits remarkable recognition sensing capability for fluoride ions among various anions, marked by its excellent selectivity and sensitivity. This is achieved through a substantial fluorescence emission enhancement, effectively operating as a "turn-on" fluorescence mechanism. The pronounced selectivity and sensitivity of complex **1** are attributed to its unique chlorine binding sites, which, through halide exchange, form tin(IV) fluoride complexes (**3**). This transformation results in distinctive fluorescence enhancement, specifically in response to fluoride ions and no other halides or tested anions. Additionally, the photophysical properties of the tin(IV) complexes were significantly influenced by the introduction of CH_3^- substitutions on hydroxyquinoline. The presence of this substituent leads to pronounced modification in bonding near the metal center owing to increased steric hindrance. Consequently, replacing Cl with F atoms enhanced complex stability and increased the dipole moment. Therefore, the exchange process is favorable relative to the other tin(IV) complexes, and the optical response to F is significant.

Conflicts of interest

The authors declare that there are no competing financial interests.

Acknowledgments

References

1   R. H. Selwitz, A. I. Ismail and N. B. Pitts, *Lancet*, 2007, **369**, 51–59.
2   S. Ayoob and A. K. Gupta, *Crit. Rev. Environ. Sci. Technol.*, 2006, **36**, 433–487.

3   J. Podgorski and M. Berg, *Nat. Commun.*, 2022, **13**, 4232.

4   M. Hirai, M. Myahkostupov, F. N. Castellano and F. P. Gabbaï, *Organometallics*, 2016, **35**, 1854–1860.

5   A. J. Malin, C. Lesseur, S. A. Busgang, P. Curtin, R. O. Wright and A. P. Sanders, *Environ. Int.*, 2019, **132**, 105012.

6   M. Boiocchi, L. Del Boca, D. E. Gómez, L. Fabbrizzi, M. Licchelli and E. Monzani, *J. Am. Chem. Soc.*, 2004, **126**, 16507–16514.

7   V. Amendola, G. Bergamaschi, M. Boiocchi, L. Fabbrizzi and L. Mosca, *J. Am. Chem. Soc.*, 2013, **135**, 6345–6355.

8   K.-J. Chang, D. Moon, M. S. Lah and K.-S. Jeong, *Angew. Chemie Int. Ed.*, 2005, **44**, 7926–7929.

9   M. Cametti and K. Rissanen, *Chem. Soc. Rev.*, 2013, **42**, 2016–2038.

10   R. Martínez-Máñez and F. Sancenón, *Chem. Rev.*, 2003, **103**, 4419–4476.

11   S. A. Khan, Q. Ullah, H. Parveen, S. Mukhtar, K. A. Alzahrani and M. Asad, *J. Photochem. Photobiol. A Chem.*, 2021, **406**, 113022.

12   B. R. Jali, A. K. Barick, P. Mohapatra and S. K. Sahoo, *J. Fluor. Chem.*, 2021, **244**, 109744.

13   A. Roy, D. Kand, T. Saha and P. Talukdar, *Chem. Commun.*, 2014, **50**, 5510–5513.

14   S. Y. Kim and J.-I. Hong, *Org. Lett.*, 2007, **9**, 3109–3112.

15   Y. Zhou, J. F. Zhang and J. Yoon, *Chem. Rev.*, 2014, **114**, 5511–5571.

16   D.-G. Cho and J. L. Sessler, *Chem. Soc. Rev.*, 2009, **38**, 1647–1662.

17   Z. Guo, I. Shin and J. Yoon, *Chem. Commun.*, 2012, **48**, 5956–5967.

18   K. M. K. Swamy, Y. J. Lee, H. N. Lee, J. Chun, Y. Kim, S. J. Kim and J. Yoon, *J. Org. Chem.*, 2006, **71**, 8626–8628.

19   D. L. Ma, V. P. Y. Ma, D. S. H. Chan, K. H. Leung, H. Z. He and C. H. Leung, *Coord. Chem. Rev.*, 2012, **256**, 3087–3113.

20   L. Fabbrizzi and A. Poggi, *Chem. Soc. Rev.*, 2013, **42**, 1681–1699.

21   L. Fabbrizzi, M. Licchelli, G. Rabaioli and A. Taglietti, *Coord. Chem. Rev.*, 2000, **205**, 85–108.

22   S. Li, C. Zhang, S. Huang, F. Hu, J. Yin and S. H. Liu, *RSC Adv.*, 2012, **2**, 4215–4219.

23   C. Parthiban, S. Ciattini, L. Chelazzi and K. P. Elango, *RSC Adv.*, 2016, **6**, 91265–91274.

24   A. K. Purohit, S. K. Padhan, J. R. Mohanty and P. K. Kar, *Photochem. Photobiol. Sci.*, 2018, **17**, 815–821.

25   A. Tarai and J. B. Baruah, *RSC Adv.*, 2015, **5**, 82144–82152.

26   K. Ngo, B. Averkiev, G. T. Reeves, A. Wu and D. W. Ki, *J. Coord. Chem.*, 2022, **75**, 796–807.

27   W. Ki, K. Ngo, P. Ghosh, B. Averkiev, G. T. Reeves, I. Ailes, B. C. Pemberton, K. Zhu and J. Li, *Chem. Commun.*, 2020, **56**, 9648–9650.

28   J. Q. Wang, Y. Mu, S. De Han, J. Pan, J. H. Li and G. M. Wang, *Inorg. Chem.*, 2019, **58**, 9476–9481.

29   Y. Kawamoto, Y. Kinoshita and H. Tamiaki, *Tetrahedron*, 2020, **76**, 130948.

30   W. White and P. G. Seybold, *J. Phys. Chem.*, 1977, **81**, 2035–2040.

31   K. M. Lo and S. W. Ng, *Acta Crystallogr. Sect. E Struct.*

32   *Reports Online*, 2009, **65**, m719.

32   *Bruker U., Apex3 v2019.1-0, SAINT V8.40A, 2019, Bruker AXS Inc.: Madison (WI), .*

33   L. Krause, R. Herbst-Irmer, G. M. Sheldrick and D. Stalke, *J. Appl. Crystallogr.*, 2015, **48**, 3–10.

34   *SHELXTL suite of programs, Version 6.14, 2000-2003, Bruker Advanced X-ray Solutions, Bruker AXS Inc., Madison, Wisconsin: USA, .*

35   G. M. Sheldrick, *Acta Crystallogr. Sect. A Found. Crystallogr.*, 2008, **64**, 112–122.

36   C. B. Hübschle, G. M. Sheldrick and B. Dittrich, *J. Appl. Crystallogr.*, 2011, **44**, 1281–1284.

37   O. V. Dolomanov, L. J. Bourhis, R. J. Gildea, J. A. K. Howard and H. Puschmann, *J. Appl. Crystallogr.*, 2009, **42**, 339–341.

38   J. R. Lakowicz, *Principles of Fluorescence Spectroscopy*, Springer US :, New York, NY :, 2nd ed. 19., 1999.

39   M. J. ea Frisch, G. W. Trucks, H. B. Schlegel, G. E. Scuseria, M. A. Robb, J. R. Cheeseman, G. Scalmani, V. Barone, G. A. Petersson and H. Nakatsuji, *Gaussian 16, revision C. 01*, Gaussian, Inc., Wallingford CT, 2016.

40   A. D. Becke, *J. Chem. Phys.*, 1993, **98**, 5648–5652.

41   T. Yanai, D. P. Tew and N. C. Handy, *Chem. Phys. Lett.*, 2004, **393**, 51–57.

42   C. Lee, W. Yang and R. G. Parr, *Phys. Rev. B*, 1988, **37**, 785–789.

43   P. J. Hay and W. R. Wadt, *J. Chem. Phys.*, 1985, **82**, 270–283.

44   C. Beattie, P. Farina, W. Levason and G. Reid, *Dalt. Trans.*, 2013, **42**, 15183–15190.

45   E. N. Keyzer, P. D. Matthews, Z. Liu, A. D. Bond, C. P. Grey and D. S. Wright, *Chem. Commun.*, 2017, **53**, 4573–4576.

46   D. Dermitzaki, C. P. Raptopoulou, V. Psycharis, A. Escuer, S. P. Perlepes and T. C. Stamatatos, *Dalt. Trans.*, 2014, **43**, 14520–14524.

47   S. M. Lee, K. M. Lo and E. R. T. Tiekink, 2019, **234**, 823–825.

48   E. Kellö, V. Vrábel, J. Holeček and J. Sivý, *J. Organomet. Chem.*, 1995, **493**, 13–16.

49   Q. Wang, *Acta Crystallogr. Sect. E Struct. Reports Online*, 2009, **65**, m905.

50   C. Zhu, Y. Wang, Q. Mao, F. Li, Y. Li and C. Chen, *Materials (Basel).*, , DOI:10.3390/ma10030313.

51   S. M. El-Megharbel and M. S. Refat, *J. Mol. Struct.*, 2015, **1085**, 222–234.

52   J. Mei, Y. Hong, J. W. Y. Lam, A. Qin, Y. Tang and B. Z. Tang, *Adv. Mater.*, 2014, **26**, 5429–5479.

53   Y. Hong, J. W. Y. Lam and B. Z. Tang, *Chem. Soc. Rev.*, 2011, **40**, 5361–5388.

54   Z. He, C. Ke and B. Z. Tang, *ACS Omega*, 2018, 3, 3267–3277.

55   Y.-R. Luo, *Comprehensive handbook of chemical bond energies*, CRC press, 2007.

56   H. A. Benesi and J. H. Hildebrand, *J. Am. Chem. Soc.*, 1949, **71**, 2703–2707.

57   X. Yang, G. Zhang, Y. Li, Z. Liu, X. Gong, B. Gao, G. Zhang, Y. Cui and G. Sun, *RSC Adv.*, 2015, **5**, 22455–22462.

58   N. Jiang, X. Gong, T. Zhong, Y. Zheng and G. Wang, *J. Mol. Struct.*, 2020, **1219**, 128573.

59   B. Mohan, K. Modi, C. Patel, S. Kumar, T. Zhiyu, H. You and P. Ren, *J. Photochem. Photobiol. A Chem.*, 2021, **408**, 113097.

60   T. Mizuno, W. H. Wei, L. R. Eller and J. L. Sessler, *J. Am. Chem. Soc.*, 2002, **124**, 1134–1135.

61   Q. Zhao, F. Li, S. Liu, M. Yu, Z. Liu, T. Yi and C. Huang, *Inorg. Chem.*, 2008, **47**, 9256–9264.